

Mesoscale distributions of UV spectral irradiance obtained by merging satellite remote sensing and ground-based measurements

Melanie A. Wetzel*^a and James R. Slusser^b

^aDivision of Atmospheric Sciences, Desert Research Institute, Reno, NV 89512

^bNatural Resources Ecology Laboratory, Colorado State University, Fort Collins, CO 80521

ABSTRACT

Global atmospheric trends in ozone column amount has focused attention on the environmental risk of exposure to ultraviolet (UV) radiation. Monitoring UV irradiance in diverse and remote locations is necessary to understand the variability of exposure, dose rates and resultant vulnerability of ecological systems. The USDA UV-B Monitoring Program maintains a wide network for ground-based continuous measurement of solar radiation in several wavelengths of interest for photosynthesis, plant growth and UV exposure to humans. This network provides data for analysis of UV climatology and trends at those sites. A satellite-based technique for producing mesoscale-resolution mapped distributions of UV spectral irradiance has been developed for extending this information into a region surrounding the network sites. The methodology combines radiative transfer modeling, multispectral image pixel classification, cloud optical depth retrievals and auxiliary remote sensing data. The results of the method are compared with ground-based measurements and utilized to examine the role of cloud distribution and surface albedo in determining mesoscale variability of UV exposure in high-latitude and high-altitude environments.

1. INTRODUCTION

Exposure to ultraviolet (UV) radiation has serious impacts on living organisms from microbes to humans¹⁻³. Most damaging are rays in the UVB (280-320 nm) wavelength region which have been linked to skin cancer^{4,5} as well as impairment of plant growth^{6,7}. Cloud cover, solar zenith angle and ozone column amount normally provide the largest degree of fluctuation in UV irradiance at the surface, and both are subject to regional and global atmospheric process trends. Depletion of stratospheric ozone as well as alterations in cloud climatology can cause significant impacts on UV irradiance^{8,9} and tropospheric chemistry¹⁰.

While extensive cloud layers reduce UV transmittance¹¹, significant doses of UV radiation can still reach the surface in the presence of cloud¹² especially for optically thin cirrus, and situations of partial cloud cover that can actually result in time periods with irradiances above clear-sky values due to scattering from cloud edges¹³. Satellite remote sensing techniques have been developed to estimate UV irradiance using measurements of upwelling ultraviolet radiances¹⁴⁻¹⁶. Use of satellite-obtained high resolution imagery offers an opportunity to monitor more precisely the spatial and temporal distribution of cloud over a location, and to study the correspondence between surface- and satellite-estimated cloud extinction¹⁷. Verdebout¹⁸ has used geostationary Meteosat and ancillary data over Europe to produce time series maps of surface UV radiation at 0.05° resolution. Meerkotter *et al.*¹⁹ used the NOAA Advanced Very High Resolution Radiometer (AVHRR) with addition of global ozone data for a case study of high-resolution surface UV mapping. The AVHRR platform is desirable for application development due to the long history (two decades) of archived data available for use in retrospective and climatological studies.

Over high latitudes, satellite image data from the geostationary environmental satellites is distorted or not available. Data that can be obtained during daylight hours by polar-orbiting satellite sensors (such as the AVHRR) varies seasonally (due to large range of day length) and also is subject to the number of operational satellites in orbit. Nevertheless, data obtained from AVHRR overpasses can be valuable in analysis of UV irradiances and for comparison with other data sources such as the NASA Total Ozone Mapping Spectrometer (TOMS). Geostationary satellite data have the advantage of high temporal resolution and thus can be used to more accurately estimate total

daily insolation. The geostationary platforms have the disadvantage of lacking coverage of high latitude regions. Thus, a procedure that can use both polar-orbiter or geostationary data is adaptable to application anywhere on the globe.

In this study, we demonstrate a procedure for using AVHRR or GOES data with surface measurements and radiative transfer modeling to map the mesoscale distribution of spectral UV irradiance over mountainous regions in Alaska and Colorado. Spectral irradiances are critical parameters in calculating biological responses to UV exposure²⁰⁻²². The primary sources of mesoscale variability include cloud distribution and surface albedo patterns^{23,24}.

2. GROUND-BASED UV MEASUREMENTS

Ground-based measurements were utilized for comparisons to model-derived spectral irradiances as well as for evaluation of the satellite-derived estimates of irradiance from the satellite datasets. The USDA UVB Monitoring and Research Network²⁵ consists of 28 US and Canadian sites and one New Zealand site which measure total horizontal, direct, and diffuse UV irradiances using the ultraviolet shadow-band radiometer (UV-MFRSR) at seven UV wavelengths: 300- 305-, 311-, 317-, 325-, 332-, and 368-nm with a full-width at half maximum of about 2.0 nm. The irradiance data are used to retrieve spectral optical depth and ozone column amount²⁶. In addition, other relevant parameters are routinely measured including visible radiation using the Vis-MFRSR²⁷, temperature, humidity, and upwelling shortwave radiation (to determine the presence of snow).

Radiometric calibration of the detectors is performed by the NOAA Central Ultraviolet Calibration Facility (CUCF) in Boulder, CO, using 1000-W NIST-traceable lamps²⁸. The spectral response of each of the radiometer's seven channels is measured by the CUCF to within an accuracy of 0.02 nm using a ISA 1.0 m double monochromator. Radiometric stability of the detectors is monitored in the field using a time series of Langley plot voltage intercepts. The approximate drift per year, determined by the least squares slope of the voltage intercept time series, is less than 10% for all channels. The angular or cosine response of the detectors is measured by Yankee Environmental System (Turners Falls, MA), and direct beam and diffuse corrections applied using the isotropic sky assumption²⁹. The total absolute radiometric uncertainty is estimated at $\pm 5.2\%$ ³⁰.

3. MESOSCALE RETRIEVAL OF SPECTRAL UV IRRADIANCE

A schematic diagram in Figure 1 illustrates the procedure for retrieval of UV spectral irradiance. Prior to the analysis of satellite data, radiative transfer modeling was carried out to prepare arrays of the range of direct and diffuse irradiances under varying conditions of surface albedo and cloud optical depth. Spectral irradiances for clear and cloudy scenes are calculated using the Santa Barbara DISORT Atmospheric Radiative Transfer (SBDART) model³¹. The code was modified to use the extraterrestrial solar flux obtained by the SUSIM spectrometer aboard the Space Shuttle Atlas 3 flight (data corrected from vacuum to air). The accuracy of this spectrum was recently validated by Grobner and Kerr³². Model input for ozone column amount was obtained from NASA TOMS database and the USDA UV-MFRSR database. Aerosol optical depth parameters were also available from the USDA database.

The procedure used either AVHRR or GOES satellite data, depending on geographic region or data availability. These satellites provide image data swaths with 5 spectral channels in the visible, near infrared and thermal infrared bands. Pixel resolution in all channels is approximately 1.1 km for AVHRR, while the GOES pixel resolution is 1 km in the visible channel but 4 km in the infrared channels used. The satellite data are remapped from pixels to a 1-km rectangular projection of dimension 300 x 300 grid cells, centered on the study sites. All cells within the study region are assigned a scene type based on multispectral analysis of the image data. The channel threshold technique is similar to the daytime classification method of Turner *et al.*³³. Gridded cell values of the visible reflectance were scaled by the solar zenith angle (SZA). Reflectance threshold values are essential for discrimination of land from

snow or cloud. Cells are classified as (non-snow) land surfaces if visible reflectance is less than specified threshold value. The Normalized Difference Vegetation Index obtained from AVHRR or other satellite platforms could be useful in assigning a vegetation reflectance for UV bands.

Reflectance in the near infrared (NIR; 3.7 or 3.9 micron band, depending on satellite) was obtained by subtracting the emitted thermal component (obtained from the radiative-equivalent temperature determined from the thermal channel image data) and then scaling the reflected radiance by the SZA. Cells that passed the visible brightness test were further classified as snow or cloud by the use of NIR threshold and thermal threshold tests. Snow and ice cloud have a low value of the NIR reflectance and a relatively warm temperature in the thermal infrared (TIR) channel. Clouds are either very bright in the NIR (if composed primarily of water droplets), or quite cold in the TIR (high ice clouds). Refinements to the pixel classification procedures can be developed from the multispectral image datasets compiled for different seasons in this locale.

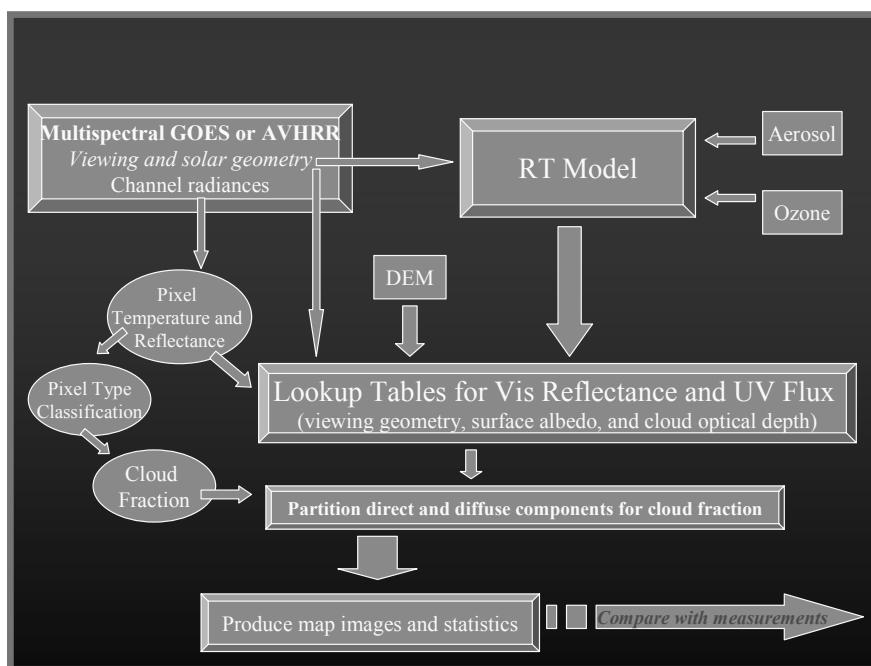


Figure 1. Schematic diagram for the production of mesoscale mapped distributions of spectral downwelling UV irradiance using GOES or AVHRR data with radiative transfer modeling.

Grid cell types determined from the classification procedure were used to assign model-derived radiative flux components at each point. First, the satellite visible channel irradiances for each grid cell were obtained by interpolation from arrays of model results for variable surface albedo (model input values beginning at 0.05 and increasing in intervals of 0.10), cloud optical depth (model values increasing from 5 to 200), satellite zenith angle (5, 15, 25,...75 degrees) and sun-satellite relative azimuth angle (increments of 30 degrees). The angle parameters are known for each grid point from the image navigation data. The UV surface albedo was assumed to equal the calculated visible reflectance based on field measurements by McKenzie *et al.*³⁴. Cloud optical depth was estimated by interpolation from visible reflectance for those pixels classified as cloudy.

If the scene at the point is designated locally cloud-free with no surrounding cloud fraction, then UV spectral flux to the point was calculated from model clear-sky irradiance adjusted for differences between control point and local conditions of estimated surface albedo. Model simulations of variations in spectral irradiance due to surface reflectance have been tabulated to allow these adjustments. Model results for increasing albedo provided an enhancement for UV irradiance caused by multiple scattering between the surface and atmosphere. In future refinements of the procedure, the grid-point surface elevation (obtained from a Digital Elevation Model gridded topographic dataset) will be used to adjust irradiance based on surface elevation (or surface air pressure). If multiple TOMS footprints exist in the study region, then this information on the spatial variability in column ozone amount can be interpolated to the mesoscale analysis grid.

Model irradiances were separated into clear-sky direct beam (E_D) and diffuse (E_d) sky components as well as cloudy-sky direct (E_{Dc}) and diffuse (E_{dc}) components, and these were used to determine the total irradiance under overcast, fully clear, or partial cloud cover conditions. When a point location was cloud-free but a non-zero cloud fraction (CF) existed in the 30-km box centered on that point (as diagnosed from cloud classification within the 30 km x 30 km surrounding area), the irradiance for that point was modified by increasing the magnitude of downward direct irradiance to account for UV direct beam radiation scattered from cloud sides, and reducing the magnitude of downward diffuse irradiance to represent the cloud-filled fraction of the surrounding sky (see Equation 1). When a point location was covered by cloud, the total irradiance to that point was calculated as the sum of direct UV irradiance transmitted through that cloud, the diffuse irradiance from the non-cloudy surrounding sky, and the diffuse irradiance from the cloud-filled sky fraction (Equation 2).

The equations used to calculate total irradiance (E_t) were thus:

$$\text{For Sun not obscured ; } E_t = E_D + E_{dc} (CF) + E_d (1-CF) \quad [1]$$

$$\text{For Sun obscured ; } E_t = E_{Dc} + E_d (1-CF) + E_{dc} (CF) \quad [2]$$

The resulting UV total irradiances for a given spectral band were mapped into the same projection as the input satellite data. Sampling the output data provided statistics on the range of UV irradiances within the study area.

4. CASE STUDIES

4.1 AVHRR data application for Central Alaska

Digital satellite digital data from the NOAA AVHRR instruments are collected over the Fairbanks region by the TeraScan groundstation system at the University of Alaska Geophysical Institute. The AVHRR digital image datasets were applied to mesoscale mapping of downward UV irradiance at the surface, using the combined approach of radiative transfer modeling and multispectral image classification. Figure 2 depicts the region of analysis and the central site location of the Poker Flat ground measurement site at Poker Flat Research Range. The study region contains snowfields, mountain, forest, valley and river surfaces. Figure 3 shows a typical scene of the mixed land cover in the vicinity of Poker Flat. A panel of the three channels used in the classification showing their individual spectral characteristics is shown in Figure 4.

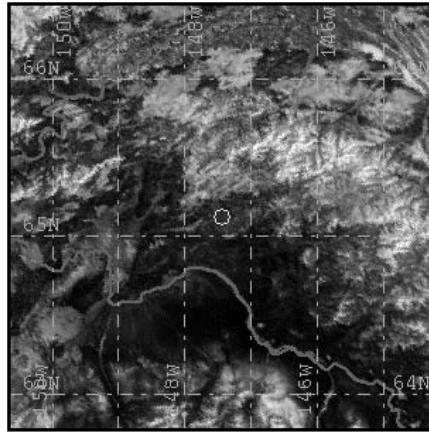


Figure 2. AVHRR visible image for a relatively clear observation time (1909 UTC on 20 April 2001) showing study region with graphic overlays of latitude/longitude grid (green), rivers (blue) and Poker Flat measurement site (yellow).



Figure 3. View from ridge overlooking Poker Flat Research Range showing typical landscape and snow cover.

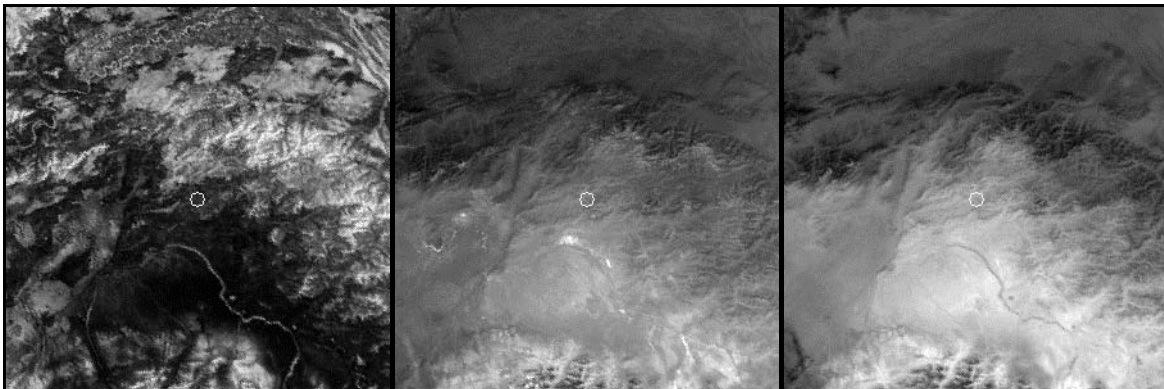


Figure 4. Panel of AVHRR multispectral imagery for 1909 UTC on 20 April in the following spectral bands: (a) visible, (b) near-infrared, and (c) thermal infrared. The circle denotes the location of the Poker Flat measurement site.

An AVHRR visible image over the study region on a day with patchy thin cirrus is shown in Figure 5. The multispectral image data and model calculations were used to estimate and map 317-nm irradiances using the method described in Section 3. The resulting gridded fields of pixel classification, cloud optical depth and irradiance are shown in Figure 6. Note that although the bands of thin cloud are difficult to distinguish in the visible image (Figure 6), the additional spectral information available in the near-infrared and thermal infrared image data allows the cloud bands to be detected and accounted for in the irradiance retrieval procedure.

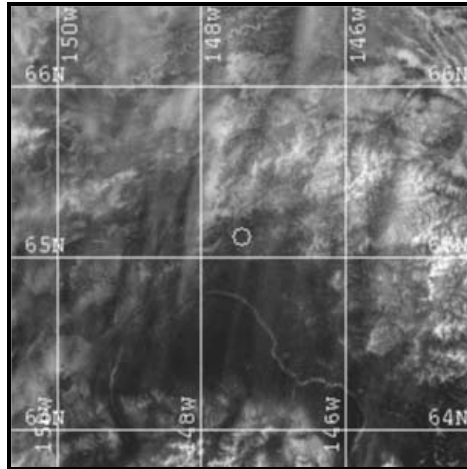


Figure 5. Visible image at 1831 UTC on 22 April 2001 indicated thin cirrus bands in study region but not obvious over Poker Flat (circle) at the observation time.

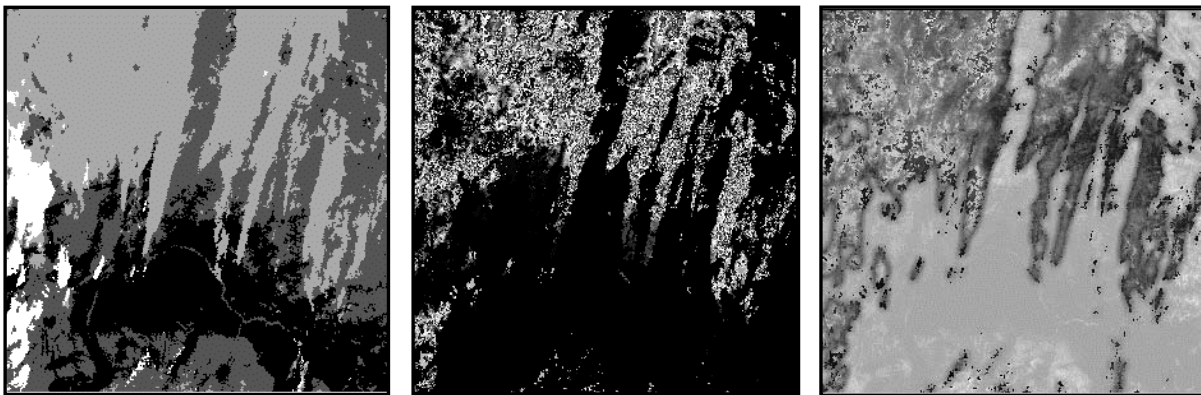


Figure 6. Results of multispectral remote sensing and model-based retrieval analysis for 1831 on 22 April 2001 over study region, showing scaled images of (a) pixel types [black=land, light grey = ice cloud, dark grey = snow, white = water cloud], (b) cloud optical depth, and (c) 317-nm irradiance.

The classification in Figure 6(a) shows the snow-covered (frozen) river course and other snow-covered terrain in the mountainous sections of the study region, as well as water cloud in the left-hand (western) portion of the study area and ice cloud bands extending north to south. Snow or land pixel reflectance is determined from surface visible reflectance for those points so classified, and within the cloudy areas, optical depth (Figure 6(b)) is determined as a function of cloud-top visible reflectance. The downward-directed UV spectral irradiance field displayed in Figure 6(c) is the end result of the pixel classification, interpolation of cloud reflectance within arrays of model results to obtain optical depth, and subsequent calculation of direct and diffuse components for clear, cloudy and partly cloudy areas surrounding each grid point. The irradiance field is smooth over the clear-sky portions of the image, mottled underneath extensive clouds due to optical depth variability, and an edge effect around the perimeter of cloudy areas is due to the scattering of radiation from nearby clouds to points that also receive direct sunlight.

Figure 7 presents a time series of ground-based observations, modeled clear-sky values and AVHRR-retrieved estimates of downward spectral irradiance for the Poker Flat site on 22 April 2001. Variations between the hourly observations and clear-sky model results are attributed to the patchy cloud cover moving over Poker Flat during the day. Results from the AVHRR-based method are close to observed values. The grid of spectral irradiances was sub-sampled over an area 100 km x 100 km centered on Poker Flat, to provide a comparison to larger-scale satellite products such as TOMS global ozone maps. The (100km)² area covers the center third of the images shown in Figures 5 and 6. Figure 8 is a histogram of irradiances calculated for this region. The majority of values lie in the range 0.07-0.08 W m⁻² nm⁻¹, closely matching the observations at 1831 UTC (0931 AST) in Figure 7. However, there is a wide range of values for the various points within the sample region, and the areal average is notably lower (0.059 W m⁻² nm⁻¹). Other parameters obtained from the analysis are shown in the legend box; there is 36% cloud cover for the region, and average cloud optical thickness is 5.2, suggesting the effect of even thin cloud on UV irradiance reaching the surface over a TOMS product footprint.

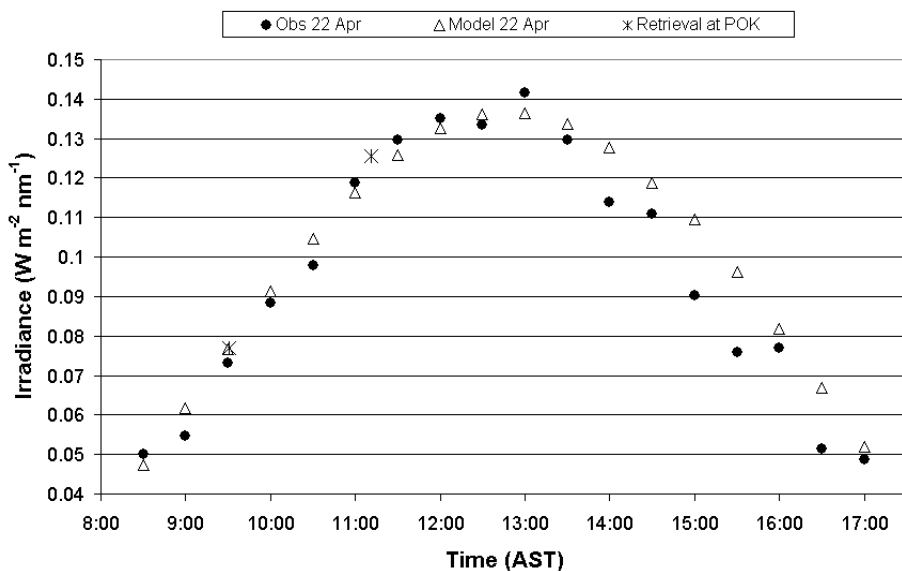


Figure 7. Observations and estimates from model and retrieval procedures for 317-nm irradiance on 22 April 2001 at Poker Flat.

Retrieval Results at 1831 UTC over TOMS FOV for Poker Flat, AK

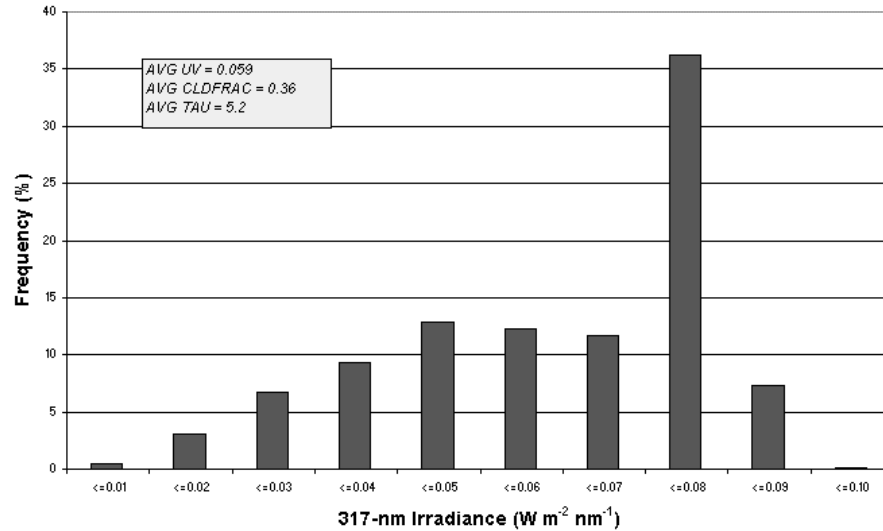


Figure 8. Histogram of irradiances for a 100km x 100 km area centered on Poker Flat (representing a typical TOMS field of view) obtained for the AVHRR observation time of 1831 UTC on 22 April 2001, using the multispectral remote sensing and model method. Each interval represents the number of points with irradiances larger than the previous interval, for example the number of points indicated in the interval <=0.08 are those with irradiance values within the range 0.07-0.08. Indicated in the legend are the average irradiance, average cloud fraction, and average cloud optical depth values estimated for that area.

4.2 GOES data application for Colorado

GOES-West satellite digital data were applied to mesoscale mapping of downward UV irradiance for a region of the central Rocky Mountains centered on the DRI Storm Peak Laboratory using the method described in Section 3. Figure 9 is a photo showing the typical terrain of this mountainous portion of this study area. The topography generally has a large influence on surface albedo (snow cover) and cloud patterns (orographically-enhanced cloud formation), as indicated by a GOES visible image (Figure 10(a)) and a topographic elevation image Figure 10(b) for the study region.



Figure 9. Photograph showing typical topographic and vegetative landscape of the higher elevation portions of the study region in central northern Colorado.

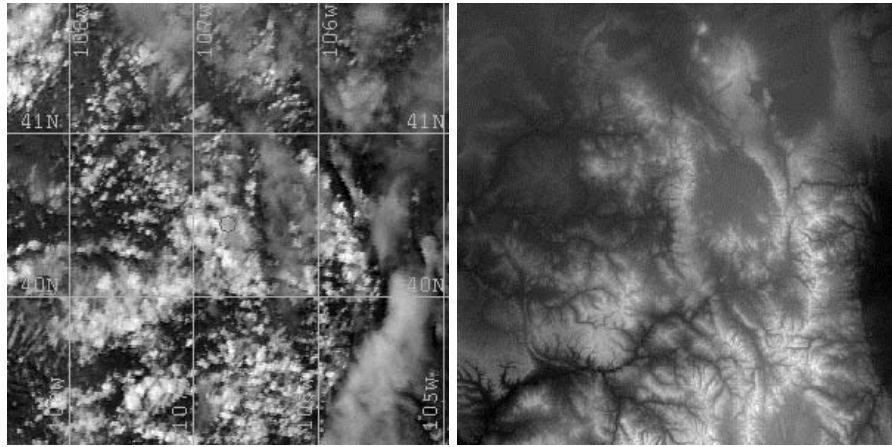


Figure 10. (a) GOES visible image of study region in central northern Colorado for 2020 UTC on 9 April 2001, showing convective and wave cloud development associated with topography, and (b) digital elevation image of study area.

The classification and radiative transfer retrieval methods were applied to image datasets over this region for multiple times and days. Figure 11 portrays the cell classification and 317-nm irradiance products for the time corresponding to Figure 10(a). The distinction between water cloud and ice cloud is indicated for the orographic convection and portions of the wave cloud areas, and some areas of snow cover are identified as well. The UV irradiance field shows significant mesoscale variability due to the effects of cloud cover, surface albedo, and the presence of surrounding cloud (adjacent pixel effects). Figure 12 indicates that the retrieved values provide very good estimates of downwelling irradiance even in the presence of full or partial cloud cover. GOES data are generally available at a 15-minute time resolution, facilitating time-specific comparisons with ground measurements and cloud conditions, analysis of time series, and calculation of time-composited parameters such as total daily spectral insolation.

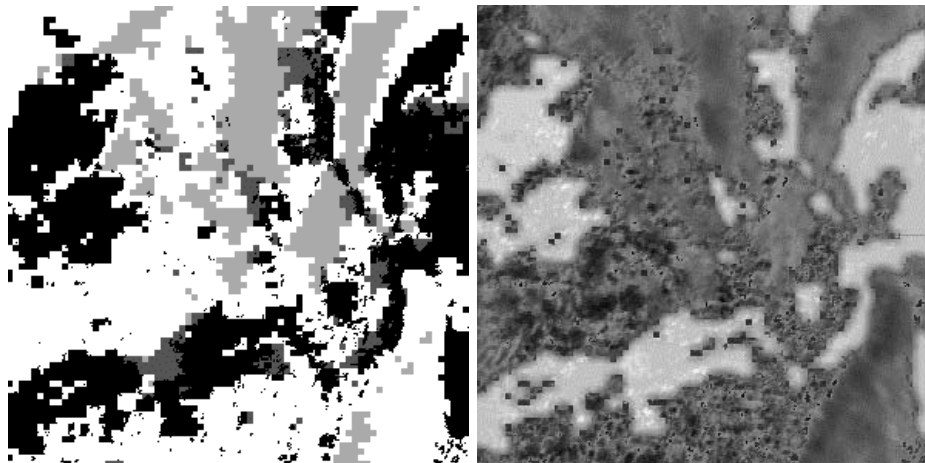


Figure 11. Results of multispectral remote sensing and model-based retrieval analysis for 2020 UTC on 9 April 2002 over study region, showing scaled images of (a) pixel types [black=land, light grey = ice cloud, dark grey = snow, white = water cloud] and (b) 317-nm downward surface irradiance.

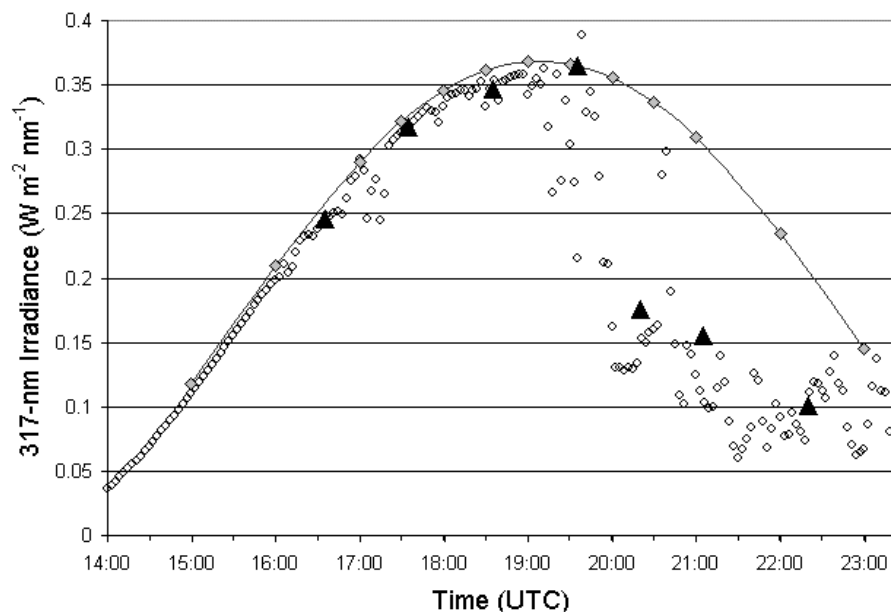


Figure 12. Retrieved estimates (triangles), clear-sky model calculations (diamonds) and measurements (circles) for 317-nm irradiance on 9 April 2002 at Strom Peak Lab.

5. CONCLUSIONS AND DISCUSSION

A new method for retrieval and mesoscale mapping of downwelling spectral irradiance has demonstrated useful accuracy when compared with ground-based measurements made at sites in mountainous locations of central Alaska and central Colorado. The results were also used to evaluate the correspondence between site-specific measurements and irradiances that might be obtained over a larger area, for example a satellite-derived product with a 100 km grid resolution. Significant enhancement can be created by locally specific conditions such as persistent snow cover or high elevation. UV irradiance climatology at high latitudes and high altitudes is an important aspect of environmental monitoring, where day length is extended, surface albedo is often high even during the summer, atmospheric attenuation is generally small, and there is a large annual cycle in ozone column amount. Use of high-resolution satellite image data in remote areas can also be applied to improving forecasts of UV exposure³⁵, with specific application to agricultural/forest workers, satellite estimation of actinic flux³⁶ for monitoring photochemical air pollution processes, and study of biogenic emissions influenced by the magnitude of absorbed UV and photosynthetically active radiation.

ACKNOWLEDGEMENTS

This research was supported by USDA, Desert Research Institute, and grants from NOAA and NSF through the International Arctic Research Consortium. The authors extend their appreciation to Gwen Scott, George Janson and Bill Durham of the Natural Resources Ecology Lab, Cathy Cahill and Glenn Shaw of the University of Alaska, and Randolph Borys of the DRI Storm Peak Laboratory.

REFERENCES

1. Frederick, J. E., and D. Lubin, "The budget of biologically active ultraviolet radiation in the Earth-Atmosphere system", *J. Geophys. Res.*, *93*, 3825-3832 1988.
2. Madronich, S., "Implications of recent total atmospheric ozone measurements for biologically active ultraviolet radiation reaching the Earth's surface," *Geophys. Res. Lett.*, *19*, 37-40, 1992.
3. Herman, J. R., B.K. Bhartia, J. Ziemke, Z. Ahmad, and D. Larko, "UV-B increases (1979-92) from decreases in total ozone", *Geophys. Res. Letter*, *23*, 2117-2120, 1996.
4. Madronich, S., and F.R. de Gruijl, "Skin cancer and UV radiation," *Nature*, *366*, 23, 1993.
5. Williams, G., and A. Green, "A cumulative-exposure model for predicting the increase in non-melanoma skin cancer associated with ozone depletion", *Cancer Forum*, *20*, 195-198, 1996.
6. Grant, R.H., "Partitioning of biologically active radiation in plant canopies." *Int. J. Biometeor.*, *40*, 26-40, 1997.
7. Caldwell, M.M., L.O. Björn, J. F. Bornman, S.D. Flint, G. Kulandaivelu, A.H. Teramura and M. Tevini, "Effects of increased solar ultraviolet radiation on terrestrial ecosystems, 1998", In: Environmental Effects of Ozone Depletion: 1998 Assessment, United Nations Environment Programme, 205pp, ISBN 92-807-1724-3 UNEP.
8. Udelhofen, P.M., P. Gies, C. Roy and W.J. Randel, "Surface UV radiation over Australia, 1979-1992: Effects of ozone and cloud cover changes on variations of UV radiation", *J. Geophys. Res.*, *104*, 19135-19159, 1999.
9. Herman, J. R., N. Krotkov, E. Celarier, D. Larko, and G. Labow, "The distribution of UV radiation at the Earth's surface from TOMS measured UV-backscattered radiances", *J. Geophys. Res.*, *104*, 12,059-12,076, 1999.
10. Madronich, S., and C. Granier, "Impact of recent total ozone changes on tropospheric ozone photodissociation, hydroxyl radicals, and methane trends," *Geophys. Res. Lett.*, *19*, 465- 467, 1992.
11. Estupinan, J.G., S. Raman, G.H. Crescenti, J.J. Streicher, and W.F. Barnard, "Effects of cloud and haze on UV-B radiation", *J. Geophys. Res.*, *101*, 16807-16816, 1996.
12. Frederick, J.E., and C. Erlick, "The attenuation of sunlight by high-latitude clouds: Spectral dependence and its physical mechanisms", *J. Atmos. Sci.*, *54*, 2813-2819, 1997.
13. Schafer, J.S., V.K. Saxena, B.N. Wenny, W. Barnard, and J.J. DeLuisi, "Observed influence of clouds on ultraviolet-B radiation", *Geophys. Res. Lett.*, *23*, 2625-2628, 1996.
14. Eck, T. F., P.K. Bhartia, and J.B. Kerr, "Satellite estimation of spectral UVB irradiance using TOMS derived total ozone and UV reflectivity", *Geophys. Res. Lett.*, *22*, 611-614, 1995.
15. Li, Z., P. Wang, and J. Cihlar, "A simple and efficient method for retrieving surface UV radiation dose rate from satellite", *J. Geophys. Res.*, *105*, 5027-5036, 2000.
16. Krotkov, N. A., J. R. Herman, P. K. Bhartia, V. Fioletov, and Z. Ahmad, "Satellite estimation of spectral surface UV irradiance 2. Effect of homogeneous clouds and snow", *J. Geophys. Res.*, *106*, 11,743-11,759, 2001.
17. Matthijsen, J., H. Slaper, and H.A.J.M. Reinen, "Reduction of solar UV by clouds: a comparison between satellite-derived cloud effects and ground-based radiation measurements", *J. Geophys. Res.*, *105*, 5069-5080, 2000.
18. Verdebout, J., "A method to generate surface UV radiation maps over Europe using GOME, Meteosat, and ancillary geophysical data", *J. Geophys. Res.*, *105*, 5049-5058, 2000.
19. Meerkötter, R., B. Wissinger, and G. Seckmeyer, "Surface UV from ERS2/GOME and NOAA/AVHRR data: A case study", *Geophys. Res. Lett.*, *24*, 1939-1942, 1997.
20. Madronich, S., *Environmental Effects of Ultraviolet (UV) Radiation*, chapter: UV radiation in the natural and perturbed atmosphere, Lewis Publisher, Boca Raton, 17-69, 1993.
21. Zeng, J., R McKenzie, K. Stamnes, M. Wineland, and J. Rosen, "Measured UV spectra compared with discrete ordinate method simulations", *J. Geophys. Res.*, *99*, 23,019-23,030, 1994.

22. Kalliskota, S., J. Kaurola, P. Taalas, J.R. Herman, E.A. Celarier, and N.A. Krotkov, "Comparison of daily UV doses estimated from Nimbus 7/TOMS measurements and ground-based spectroradiometric data", *J. Geophys. Res.*, *105*, 5059-5067, 2000.
23. Herman, J. R. , and E. Celarier, "Earth surface reflectivity at 340-380 nm from TOMS data", *J. Geophys. Res.*, *102*, 28,003-28,011, 1997.
24. Krotkov, N.A., P.K. Bhartia, H.R. Herman, V. Fioletov, and J. Kerr, "Satellite estimation of spectral surface UV irradiance in the presence of tropospheric aerosols, 1. cloud-free case", *J. Geophys. Res.*, *103*, 8779-8793, 1998.
25. Bigelow, D. S., J. R. Slusser, A. F. Beaubien, and J. H. Gibson, "The USDA Ultraviolet Radiation Monitoring Program", *Bull. Amer. Meteor. Soc.*, *79*, 601-615, 1998.
26. Gao, W., J. Slusser, J. Gibson, G. Scott, D. Bigelow, J. Kerr, and B. McArthur, "Direct-Sun column ozone retrieval by the ultraviolet multifilter rotating shadowband radiometer and comparison with those from Brewer and Dobson spectrophotometers", *Appl. Opt.*, *40*, 3149-3155, 2001.
27. Harrison, L., and J. Michalsky, "Objective algorithms for the retrieval of optical depths from ground-based measurements", *Appl. Opt.*, *33*, 5126-5132, 1994.
28. Slusser, J. R., J. H. Gibson, D. Kolinski, P. Disterhoft, K. Lantz and A. F. Beaubien, "Langley Method of Calibrating UV Filter Radiometers", *J. Geophys. Res.*, 4841-4849, *105*, 2000.
29. Gröbner, J., M. Blumthaler, and W. Ambach, "Experimental investigation of spectral global irradiance measurements errors due to non-ideal cosine response", *Geophys. Res. Letts.*, *23*, 2493-2496, 1996.
30. Slusser, J.R., N. Krotkov, W. Gao, J.R. Herman, G. Labow and G. Scott, "Comparisons of USDA UV shadow-band irradiance measurements with TOMS satellite and DISORT model retrievals under all sky conditions", *Proc. SPIE*, *4482*, 56-63, 2002.
32. Gröbner, J., and J. Kerr, "Ground-based determination of the spectral ultraviolet extraterrestrial solar irradiance: Providing a link between space-based and ground-based solar UV measurements", *J. Geophys. Res.*, *106*, 7211-7217, 2001.
31. Ricchiazzi, P., S. Yang, C. Gautier, and D. Soble, "SBDART: A research and teaching software tool for plane-parallel radiative transfer in the Earth's atmosphere", *Bull., Amer. Meteor., Soc.*, *79*, 2101-2114, 1998.
33. Turner, J., G.J. Marshall, and R.S. Ladkin, "An operational, real-time cloud detection scheme for use in the Antarctic based on AVHRR data", *Int. J. Rem. Sens.*, *22*, 3027-3046, 2001.
34. McKenzie, R. L., M. Kotkamp, W. Ireland, "Upwelling UV spectral irradiances and surface albedo measurements at Lauder, New Zealand", *Geophys Res Letts.*, *23*, 1757-1760, 1996.
35. Long, C.S., A.J. Miller, H.T. Lee, J.D. Wild, R.C. Przywarty, and D. Hufford, "Ultraviolet Index forecasts issued by the National Weather Service," *Bull. Amer. Meteor. Soc.*, *77*, 729-747, 1996.
36. Mayer, B., C.A. Fischer, and S. Madronich, "Estimation of surface actinic flux from satellite (TOMS) ozone and cloud reflectivity measurements," *Geophys. Res. Letts.*, *25*, 4321-4324, 1998.